Journal of the Mechanics and Physics of Solids 000 (2020) 104099

Contents lists available at ScienceDirect

Journal of the Mechanics and Physics of Solids

journal homepage: www.elsevier.com/locate/jmps

On the effect of the loading apparatus stiffness on the equilibrium and stability of soft adhesive contacts under shear loads

A. Papangelo[a,b,*], G. Cricrì[c], M. Ciavarella[a,b]

[a] Politecnico di Bari, Department of Mechanics Mathematics and Management, Via Edoardo Orabona 4, Bari 70125, Italy
[b] Hamburg University of Technology, Department of Mechanical Engineering, Am Schwarzenberg-Campus 1, Hamburg 21073, Germany
[c] Università di Napoli Federico II, Department of Industrial Engineering, Piazzale Vicenzo Tecchio 80, Napoli 80125, Italy

ARTICLE INFO

Article history:
Received 20 February 2020
Revised 20 June 2020
Accepted 22 July 2020
Available online xxx

Keywords:
Adhesion
Friction
Mode-mixity
Fracture mechanics
Contact mechanics

ABSTRACT

The interaction between contact area and frictional forces in adhesive soft contacts is receiving much attention in the scientific community due to its implications in many areas of engineering such as surface haptics and bioinspired adhesives. In this work, we consider a soft adhesive sphere that is pressed against a rigid substrate and is sheared by a tangential force where the loads are transferred to the sphere through a normal and a tangential spring, representing the loading apparatus stiffness. We derive a general linear elastic fracture mechanics solution, taking into account also the interaction between modes, by adopting a simple but effective mixed-mode model that has been recently validated against experimental results in similar problems. We discuss how the spring stiffness affects the stability of the equilibrium contact solution, i.e. the transition to separation or to sliding.

1. Introduction

The interaction between adhesion and friction represents a very fundamental problem in tribology, particularly following the recent development of engineering systems at small scales, since surface forces such as adhesion and friction become stronger than volume forces (Argatov et al., 2020; Argatov and Papangelo, 2019; Bhushan et al., 1995; Ciavarella, 2018; Ciavarella et al., 2019; Ciavarella and Papangelo, 2017; Heim et al., 1999; Homola et al., 1990; Pelesko and Bernstein, 2002; Ciavarella, Papangelo, Afferrante, 2017; McMeeking et al., 2020; Lengiewicz, de Souza, Lahmar, Courbon, Dalmas, Stupkiewicz, Scheibert).

Adhesion and friction are important in systems involving soft materials, investigated since the early work of Savkoor and Briggs (1977) who extended the Johnson-Kendall-Roberts model (JKR, Johnson et al., 1971) to account for a tangential force. Savkoor and Briggs (1977) treated the contact as an external crack under mode-mixity, i.e. experiencing on the contact patch periphery mode I (opening), due to short-range adhesion, and mode II and III (respectively in- and anti-plane shearing) due to the tangential force applied. Their model is "purely-brittle" in the sense that any dissipative phenomena coming from the frictional interaction were neglected. As a result it overestimated the contact area reduction when compared with experiments.

* Corresponding author.
E-mail address: antonio.papangelo@poliba.it (A. Papangelo).

https://doi.org/10.1016/j.jmps.2020.104099
0022-5096/

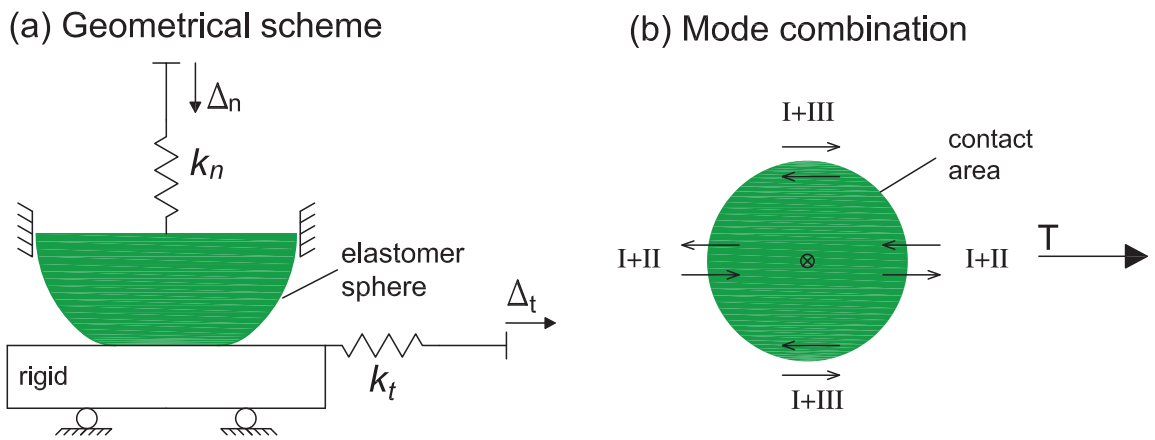

Fig. 1. (a) An elastic sphere squeezed against a flat and rigid substrate. Δ_n (Δ_t) is the normal (tangential) displacement imposed at the free end of the normal (tangential) spring. The contact patch sticks to the substrate and (b) shrinks circularly under mixed-mode loading conditions.

This is intimately related to fracture of bimaterial interfaces under mixed-mode loading, where various authors (Cao and Evans, 1989; Hutchinson, 1990; Hutchinson and Suo, 1992) have indicated that the apparent "toughness" of an interface strongly depends on the phase angle $\psi = \arctan(K_{II}/K_I)$, being K_{II} and K_I the stress intensity factors under mode II and mode I. One way to deal with this is adding a phenomenological mode-mixity function $f(\psi)$ to account for the dissipative effects happening at the interface, such as friction, plasticity and dislocations. Hence, the equilibrium condition is written as

$$G = G_c = G_{Ic} f(\psi) \tag{1}$$

where G is the energy release rate, G_c is its critical value for crack propagation (interfacial toughness) and G_{Ic} is the critical energy release rate under pure opening conditions. Hutchinson and Suo (1992) proposed different forms for $f(\psi)$, which have been used by different authors in the contact mechanics context (Argatov and Papangelo, 2019; Johnson, 1996; 1997; Papangelo and Ciavarella, 2019; Sahli et al., 2018; 2019; Waters and Guduru, 2010) for an adhesive sphere under a shear load. Recently Papangelo, Scheibert, Sahli, Pallares, Ciavarella (2019) extended the approximate JKR solution for elliptical contacts by Johnson and Greenwood (2005) to include the effect of the tangential force, which allowed to accurately predict not only the size of the contact patch, but also its shape (see also Argatov et al., 2020).

So far, all the theoretical studies on this topic we just mentioned, have assumed that the normal and tangential forces are directly applied to the soft sphere neglecting the inherent stiffness of the loading system and/or of the bulk material. In a typical experimental test-rig, the normal and tangential loads are applied through a cantilever that acts as a two-dimensional force transducer introducing a certain normal and tangential stiffness as sketched in Fig. 1a (compare also Fig. 4 in Waters and Guduru (2010) or Fig. 2 in Mergel et al. (2018)). For example, Waters and Guduru (2010) report that the loading system introduces a normal and tangential stiffness respectively equal to 1.69 N/mm and 3.76 N/mm. Assuming that the contact patch is in full stick, the normal and tangential stiffness of the contact can be estimated as $2aE^* \simeq 2.3$ N/mm and $4/3aE^* \simeq 1.5$ N/mm (Maugis, 2000)), where, from Waters and Guduru (2010), $a = 0.5$ mm is a typical value for the contact radius and $E^* = 2.3$ N/mm^2 is the composite elastic modulus. Hence, the stiffness of the measuring system was comparable with that of the contact patch.

In this work, we consider the adhesive contact of a soft sphere which is loaded by imposing a normal (tangential) displacement to the free end of a normal (tangential) spring, which has the other end connected to the sphere (substrate). We derive the mechanical model from energy considerations and study how the contact area decays while increasing the imposed tangential displacement "Δ_t" for varying normal "k_n" and tangential "k_t" stiffness and imposed normal displacement "Δ_n" (see Fig. 1a). The condition for the equilibrium solutions to be stable are derived for imposed normal and tangential displacements, which may be of interest in practical experiments. We find that the contact decay is bounded between two limits that are obtained for relatively "very soft" or "very hard" springs compared with the sphere stiffness and that the "effective" (or "apparent") interface toughness depends on both the tangential displacement Δ_t and stiffness k_t (Fig. 1a).

The model which will be presented here is based on the Linear Elastic Fracture Mechanics theory, hence, as such, for mixed mode loading, loses some effectiveness with respect to the standard JKR-Griffith theory. The problem is not so much the modeling of friction as fracture, but that mixed mode loading requires ad hoc phase-dependent definitions of toughness, or else independent measurement of irreversible losses due to friction. Also, the model does not account for nonlinear effects such us large deformations (Lengiewicz et al., 2020)). Nevertheless, in the range of "low normal loads", adhesion plays a fundamental role and its contribution cannot be neglected (see Fig. 13c in Mergel et al. (2020)). Understanding the relative importance of adhesion and nonlinear deformation in contact area shrinking is still an open question (Mergel et al., 2020)), which will be addressed elsewhere.

2. Sphere-substrate contact model

2.1. Mechanical model

The model considered consists of an elastic soft sphere of radius R that is squeezed against a flat substrate. We assume short-range adhesion at the interface, so that the Johnson-Kendall-Roberts model (JKR, Johnson et al., 1971) can be adopted. It is assumed that the soft sphere is connected in the vertical direction to a normal spring of stiffness k_n and, in the horizontal direction, to a tangential spring of stiffness k_t that is connected to the substrate. Normal and tangential loads are applied to the sphere by imposing a vertical Δ_n and horizontal Δ_t displacement at the free ends of the springs k_n and k_t (see Fig. 1a). The spring k_n and the elastic sphere sustain the same normal load P as they are placed in series, hence by imposing a normal displacement Δ_n at the free end of the vertical spring we get

$$\begin{cases} \Delta_n = v + v_s \\ v_s = \dfrac{P}{k_n} \\ v = \dfrac{P}{2aE^*} + \dfrac{a^2}{3R} \end{cases} \rightarrow \begin{cases} v_s = \dfrac{2E^*a}{k_n}\left(\Delta_n - \dfrac{a^2}{3R}\right)\left(1 + \dfrac{2E^*a}{k_n}\right)^{-1} \\ v = \left(\Delta_n - \dfrac{2E^*a}{k_n}\dfrac{a^2}{3R}\right)\left(1 + \dfrac{2E^*a}{k_n}\right)^{-1} \end{cases} \tag{2}$$

where v_s is the deformation of the normal spring, v is the normal elastic displacement of the sphere within the JKR assumptions (Maugis (2000), eq. (4.147)), a is the contact radius, $E^* = \left(\frac{1-\nu_1^2}{E_1} + \frac{1-\nu_2^2}{E_2}\right)$ is the composite elastic modulus, E_i, ν_i are the Young modulus and Poisson ratio of the sphere and of the substrate. In the following, it is assumed that the substrate is rigid ($E_2 \rightarrow +\infty$) and the material of the sphere incompressible ($\nu_1 = 1/2$) so that the normal and the tangential displacement fields are uncoupled. By using Eq. (2), we obtain

$$P = 2aE^*\left(1 + \frac{2aE^*}{k_n}\right)^{-1}\left(\Delta_n - \frac{a^2}{3R}\right) \tag{3}$$

Let us impose a tangential displacement Δ_t to the free end of the horizontal spring (Fig. 1 (a)). We assume that the contact area sticks to the rigid substrate and remains axisymmetric while shrinking. The friction force at the sphere-substrate surface is equal in magnitude to the force T transmitted to the tangential spring k_t, hence

$$\begin{cases} \Delta_t = u + u_s \\ u_s = \dfrac{T}{k_t} \\ u = \dfrac{3T}{4aE^*} \end{cases} \rightarrow \begin{cases} u_s = \dfrac{4E^*a}{3k_t}\left(1 + \dfrac{4E^*a}{3k_t}\right)^{-1}\Delta_t \\ u = \left(1 + \dfrac{4E^*a}{3k_t}\right)^{-1}\Delta_t \end{cases} \tag{4}$$

where u is the uniform tangential displacement within the loaded circle and u_s is the deformation of the tangential stiffness. Notice that a uniform tangential displacement in a circular patch gives rise to a singular distribution of shear tractions (see the results in Johnson (1985), ch. 3.7). By using Eq. (4) we obtain

$$T = \frac{4E^*a}{3}\left(1 + \frac{4E^*a}{3k_t}\right)^{-1}\Delta_t \tag{5}$$

2.2. Equilibrium solutions of the system

The elastic energy of the system U is written as

$$U = U_n + U_t \tag{6}$$

where U_n and U_t are the contributions to the elastic energy in the normal and tangential direction respectively, which are obtained taking into account the deformation of the springs and of the elastic body (Maugis, 2000)

$$U_n = E^*\left(av^2 - \frac{2va^3}{3R} + \frac{a^5}{5R^2}\right) + \frac{1}{2}k_n(\Delta_n - v)^2 \tag{7}$$

$$U_t = \frac{2}{3}E^*au^2 + \frac{1}{2}k_t(\Delta_t - u)^2 \tag{8}$$

By introducing a set of auxiliary variables

$$\begin{cases} \chi = \dfrac{a^2}{R}\left(1 + \dfrac{4E^*a}{3k_n}\right) \\ \rho_n = 1 + \dfrac{2E^*a}{k_n} \\ \rho_t = 1 + \dfrac{4E^*a}{3k_t} \end{cases} \tag{9}$$

and using (2,4) we obtain

$$U(a,\Delta_n,\Delta_t)=E^*a\left[\frac{1}{\rho_n}\left(\Delta_n-\frac{a^2}{3R}\right)^2+\frac{4}{5}\left(\frac{a^2}{3R}\right)^2+\frac{2}{3}\frac{\Delta_t^2}{\rho_t}\right] \tag{10}$$

Using a well-known standard method, the energy release rate can be evaluated by calculating the partial derivative of the elastic energy (10) by the contact area $A=\pi a^2$

$$G=\frac{\partial U}{\partial A}=\frac{E^*}{2\pi a}\left[\left(\frac{\Delta_n-\chi}{\rho_n}\right)^2+\frac{2}{3}\left(\frac{\Delta_t}{\rho_t}\right)^2\right] \tag{11}$$

In the context of the fracture mechanics, G is interpreted as the energy allowable for increasing the crack surface (or decreasing the contact surface, in adhesion problems) per unit area. On the other hand, the (unit) area change implies that an energy cost must be paid in terms of surface energy; thus, a unit area decrease provokes a (tendential) passage from the volume energy U to the surface one U_s.

The energy balance requires:

$$G=\frac{\partial U}{\partial A}\le\frac{\partial U_s}{\partial A}=G_c \tag{12}$$

where, in adhesion models (or in fracture mechanics when $dA>0$), the strict equality holds. If U is classically interpreted as the free energy at imposed displacements, G will be naturally interpreted as the thermodynamic variable dual of the contact area A; in this framework, Eq. (12) barely represents the (thermodynamic) equilibrium condition for the variable A.

It is not trivial, in general, to separate G into normal and tangential sliding modes. Fortunately, in the present model, they are completely uncoupled so that one can write unambiguously:

$$G_I=\frac{\partial U_n}{\partial A}=\frac{E^*}{2\pi a}\left(\frac{\Delta_n-\chi}{\rho_n}\right)^2;\quad G_{II}=\frac{\partial U_t}{\partial A}=\frac{E^*}{3\pi a}\left(\frac{\Delta_t}{\rho_t}\right)^2 \tag{13}$$

Both in fracture mechanics and in adhesion, most of the experimental outcomes show that the surface energy rate G_c has a constant value only in the limit case of brittle behavior. More generally, it depends, among other parameters, from the mixity of the loading mode. Following a well-established standard fracture mechanics model, a simple and useful mixed-mode fracture criterion Da Silva and Öchsner (2008) is:

$$\frac{G_I}{G_{Ic}}+\frac{G_{II}}{G_{IIc}}=1 \tag{14}$$

where G_{Ic}, G_{IIc} are material constants representing, respectively, the opening and the sliding mode fracture toughness.

Note that the surface energy is now depending on the couple of constants G_{Ic}, G_{IIc} instead of the single one G_c. It may be argued that Eq. (14) cannot be considered a pure energetic equilibrium like (12), since the unitary energy G is split into two contributions with different weights. Nevertheless, this criterion and similar others are widely used in engineering applications (Da Silva and Öchsner, 2008).

From Eq. (14) one can derive:

$$G_I+\lambda G_{II}=G_{Ic};\quad \lambda=\frac{G_{Ic}}{G_{IIc}} \tag{15}$$

If one defines a "reversible" energy release rate G_{rev} and a "irreversible" one G_{irr}

$$G_{rev}=G_I+\lambda G_{II};\quad G_{irr}=(1-\lambda)G_{II} \tag{16}$$

the condition that allows to evaluate the contact area at equilibrium becomes similar to the expression (14)

$$G_{rev}=G_{Ic} \tag{17}$$

while G_{irr} represents a unit surface energy quota needed for some unspecified irreversible processes occurring at the interface during the contact area (potential) change, but not directly involved in the equilibrium of A.

Thus, the mixed-mode equilibrium criterion requires:

$$\frac{E^*}{2\pi a}\left[\left(\frac{\Delta_n-\chi}{\rho_n}\right)^2+\frac{2}{3}\lambda\left(\frac{\Delta_t}{\rho_t}\right)^2\right]=G_{Ic} \tag{18}$$

or using (9)

$$\Delta_n=\left(\frac{1}{2aE^*}+\frac{1}{k_n}\right)\left[\frac{4E^*a^3}{3R}-\sqrt{8E^*a^3\pi G_{I,eff}}\right]+\frac{a^2}{3R} \tag{19}$$

where

$$G_{I,eff} = G_{Ic} - \lambda \frac{E^*}{3\pi a}\left(\frac{\Delta_t}{1+\frac{4}{3}\frac{E^* a}{k_t}}\right)^2 \tag{20}$$

should be interpreted as an effective work of adhesion. If $k_t \to 0$, then any Δ_t would give rise to a null tangential force T, hence the problem would reduce to the classical JKR problem with a normal stiffness k_n and $G_{I,eff} = G_{Ic}$.. The same result is obtained obviously by imposing $\Delta_t = 0$. On the other hand, for $k_t \to +\infty$ the shearing force will be completely defined by the contact stiffness of the sphere and $G_{I,eff} = G_{Ic} - \lambda \frac{E^*}{3\pi a}\Delta_t^2$, which gives the greatest reduction of the effective work of adhesion with Δ_t that could be achieved and, for $\lambda = 1$, corresponds to the brittle model of Savkoor and Briggs (1977). One can easily obtain the limit condition at which $G_{I,eff} = 0$, i.e. from Eq. (20)

$$G_{Ic} = \lambda \frac{E^*}{3\pi a}\left(\frac{\Delta_t}{\rho_t}\right)^2 \tag{21}$$

which substituted into Eq. (19) and using Eq. (3) gives the Hertzian solution

$$P = \frac{4E^* a^3}{3R} \tag{22}$$

The present mixity model is equivalent to the equilibrium condition (1) when using for the mode mixity function

$$f(\psi) = \left[1 + (\lambda - 1)\sin^2(\psi)\right]^{-1} \tag{23}$$

which was first proposed by Hutchinson and Suo (1992) and that has been recently validated against experimental results by Papangelo and Ciavarella (2019). An alternative derivation of the equilibrium Eq. (19) based on the concept of Stress Intensity Factors (SIFs) is proposed in Appendix A.

3. Stability of the equilibrium solutions

Since, in this model, both G_{Ic} and λ are constants, it is licit to derive the stability condition from Eq. (15) by imposing the usual condition on the derivative of G_{rev}:

$$\frac{\partial G_{rev}}{\partial A} > 0 \Leftrightarrow \frac{\partial G_I}{\partial A} + \lambda \frac{\partial G_{II}}{\partial A} > 0 \tag{24}$$

The stability of the equilibrium solutions at fixed Δ_n and Δ_t requires

$$\frac{\partial G_{rev}}{\partial A} > 0 \Longleftrightarrow \left(a\frac{\partial^2 U_n}{\partial a^2} - \frac{\partial U_n}{\partial a}\right) + \lambda\left(a\frac{\partial^2 U_t}{\partial a^2} - \frac{\partial U_t}{\partial a}\right) > 0 \tag{25}$$

After some algebra, the stability condition (Eq. (25)) can be reduced to

$$\left(\frac{2}{\rho_n} - 3\right)\left(\frac{\Delta_n - \chi}{\rho_n}\right)^2 + \frac{4a^2}{R}\left(\frac{\chi - \Delta_n}{\rho_n}\right) + \frac{2}{3}\lambda\left(\frac{2}{\rho_t} - 3\right)\left(\frac{\Delta_t}{\rho_t}\right)^2 > 0 \tag{26}$$

Notice that, in both the equilibrium (18) and stability Eq. (26), the mixed-mode parameter λ appears always multiplied by the remote tangential displacement squared Δ_t^2, hence, we define a new variable

$$\Delta_{t,rev} = \sqrt{\lambda}\Delta_t \tag{27}$$

as the "reversible part" of the tangential displacement, which effectively governs the problem in the tangential direction.

The critical state at which the system loses its stability can be found by using the equilibrium Eq. (18) together with the stability condition Eq. (26)), where the inequality sign is substituted by the equality sign " = ". For example, for a given Δ_t, by using Eq. (18), (26) one finds the critical normal displacement and contact area ($\Delta_{n,c}$, a_c). In the figures which follow we will use solid (dashed) lines to identify stable (unstable) branches.

Notice that our results on the critical load for stability include also (but are not limited to) the transition to sliding. Here, recent experimental results by Sahli et al. (2018) suggest that, in their experiments, transition to sliding happens when a critical shear force is reached equal to $\pi a^2 \tau_0$ (where τ_0 is the shear strength at the interface), but this type of critical condition should be easily added as a competitive mechanism to the one discussed in the present paper (see Papangelo and Ciavarella, 2019).

3.1. Particular cases

It is useful to simplify the analysis for the case of very compliant or very hard springs, which coincides respectively with the cases of "load controlled" or "displacement controlled" experiments. In these limit cases Eq. (18), (26) can be simplified or solved explicitly as reported below:

1. In the limit of $k_n = k_t \to +\infty$ (displacement control in both normal and tangential directions), Eq. (18), (26) reduces to

$$\begin{cases} \Delta_c n = \dfrac{a^2}{R}\left(1 - \dfrac{\pi G_{Ic} R^2}{2E^* a^3}\right) \\ \Delta_t = \pm\sqrt{\dfrac{3\pi a G_{Ic}}{\lambda E^*}\left(1 - \dfrac{\pi G_{Ic} R^2}{8E^* a^3}\right)} \end{cases} \tag{28}$$

so that for a given Δ_t one can obtain a_c from Eq. (28, 2nd) and $\Delta_{n,c}$ from eq. (28, 1st). If $\Delta_t = 0$ Eq. (28) give the critical state of the classical JKR solution at "fixed-grips" (Maugis (2000), pag. 272)

$$\begin{cases} a_c = \left(\dfrac{\pi G_{Ic} R^2}{8E^*}\right)^{1/3} \\ \Delta_{n,c} = -\dfrac{3}{R}\left(\dfrac{\pi G_{Ic} R^2}{8E^*}\right)^{2/3} \\ P_c = -\dfrac{5}{6}\pi G_{Ic} R \end{cases} \tag{29}$$

2. In the limit of $k_n = k_t \to 0$ (load control in both normal and tangential directions) it is more convenient to use Eq. (3), (5) so that the critical condition is written in terms of forces (P, T) as the imposed displacements become ill-defined. By substituting Eq. (3), (5) into (18,26) the critical condition is written as

$$\begin{cases} P = \dfrac{4E^* a^3}{3R} - 3\pi R G_{Ic} \\ T = \pm\dfrac{4E^* a}{3}\sqrt{\dfrac{1}{\lambda}\left(\dfrac{3\pi a G_{Ic}}{E^*} - \dfrac{3}{2}\left(\dfrac{3\pi G_{Ic} R}{2aE^*}\right)^2\right)} \end{cases} \tag{30}$$

that for any tangential load T gives the critical radius of contact a_c and normal load P_c

$$\begin{cases} a_c = \left(\dfrac{9\pi G_{Ic} R^2}{8E^*} + \dfrac{3\lambda T^2}{16\pi G_{Ic} E^*}\right)^{1/3} \\ P_c = -\dfrac{3}{2}\pi G_{Ic} R + \dfrac{\lambda T^2}{4\pi R G_{Ic}} \end{cases} \tag{31}$$

If $T = 0$ the critical state of the classical JKR solution at "fixed-load" (Maugis (2000), pag. 271) is obtained

$$\begin{cases} a_c = \left(\dfrac{9\pi G_{Ic} R^2}{8E^*}\right)^{1/3} \\ P_c = -\dfrac{3}{2}\pi G_{Ic} R \end{cases} \tag{32}$$

3. In the limit of $k_n \to 0$, $k_t \to +\infty$ (load control in the normal direction, displacement control in the tangential direction) the critical condition can be written as

$$\begin{cases} P = -\sqrt{\dfrac{4E^* a^3}{3R}\left[\dfrac{10E^* a^3}{3R} - 3\pi R G_{Ic} + 2\sqrt{\dfrac{E^* a^3}{R}\left(\dfrac{E^* a^3}{R} - \pi R G_{Ic}\right)}\right]} \\ \Delta_t = \pm\dfrac{1}{\sqrt{\lambda}}\sqrt{\dfrac{9\pi a G_{Ic}}{2E^*} - 3\left(\dfrac{a^2}{R}\right)^2 - 3\dfrac{a^2}{R}\sqrt{\left(\dfrac{a^2}{R}\right)^2 - \dfrac{\pi a G_{Ic}}{E^*}}} \end{cases} \tag{33}$$

It is easily verified that Eq. (33) reduces to Eq. (32) if $\Delta_t = 0$.

4. In the limit of $k_n \to +\infty$, $k_t \to 0$ (displacement control in the normal direction, load control in the tangential direction) the critical condition can be written as

$$\begin{cases} \Delta_n = \dfrac{a^2}{R} - \sqrt{\dfrac{3\pi a G_{Ic}}{E^*} + 2\left(\dfrac{a^2}{R}\right)^2 - 2\dfrac{a^2}{R}\sqrt{\left(\dfrac{a^2}{R}\right)^2 - \dfrac{3\pi a G_{Ic}}{E^*}}} \\ T = \pm\dfrac{1}{\sqrt{\lambda}}\sqrt{\dfrac{16E^* a^3}{3R}\left[-\dfrac{E^* a^3}{R} - \dfrac{\pi}{2}R G_{Ic} + \sqrt{\dfrac{E^* a^3}{R}\left(\dfrac{E^* a^3}{R} + 3\pi R G_{Ic}\right)}\right]} \end{cases} \tag{34}$$

It is easily verified that Eq. (34) reduces to Eq. (29) if $T = 0$.

4. More results

4.1. Dimensionless notation

We will present the results in a dimensionless form. By introducing the following dimensionless notation (as firstly introduced by Maugis, 2000)

$$\xi = \left(\frac{E^* R}{G_{Ic}}\right)^{1/3}; \quad \tilde{a} = \frac{\xi a}{R}; \quad \tilde{\Delta}_t = \frac{\Delta_t \xi^2}{R}; \quad \tilde{\Delta}_{t,rev} = \sqrt{\lambda}\tilde{\Delta}_t; \quad \tilde{\Delta}_n = \frac{\Delta_n \xi^2}{R}; \tag{35}$$

$$\tilde{P} = \frac{P}{RG_{Ic}}; \quad \tilde{k}_t = \frac{\xi k_t}{RE^*}; \quad \tilde{u} = \frac{\xi^2 u}{R}; \quad \tilde{k}_n = \frac{\xi k_n}{RE^*}; \quad \tilde{G}_{I,eff} = \frac{G_{I,eff}}{G_{Ic}}; \tag{36}$$

$$\tilde{\chi} = \frac{\xi^2 \chi}{R} = \tilde{a}^2\left(1 + \frac{4\tilde{a}}{3\tilde{k}_n}\right); \quad \tilde{\rho}_n = 1 + \frac{2\tilde{a}}{\tilde{k}_n}; \quad \tilde{\rho}_t = 1 + \frac{4\tilde{a}}{3\tilde{k}_t}; \tag{37}$$

hence the equilibrium Eq. (18) is written in dimensionless form as

$$\left[\left(\frac{\tilde{\Delta}_n - \tilde{\chi}}{\tilde{\rho}_n}\right)^2 + \frac{2}{3}\left(\frac{\tilde{\Delta}_{t,rev}}{\tilde{\rho}_t}\right)^2\right] = 2\pi\tilde{a} \tag{38}$$

while the stability condition is written as

$$\left(\frac{2}{\tilde{\rho}_n} - 3\right)\left(\frac{\tilde{\Delta}_n - \tilde{\chi}}{\tilde{\rho}_n}\right)^2 + 4\tilde{a}^2\left(\frac{\tilde{\chi} - \tilde{\Delta}_n}{\tilde{\rho}_n}\right) + \frac{2}{3}\left(\frac{2}{\tilde{\rho}_t} - 3\right)\left(\frac{\tilde{\Delta}_{t,rev}}{\tilde{\rho}_t}\right)^2 > 0 \tag{39}$$

4.2. Equilibrium solutions

Let us show in Fig. 2 the relation between the dimensionless contact radius $\tilde{a}$ and the normal displacement $\tilde{\Delta}_n$ for different values of the parameters $\tilde{\Delta}_{t,rev}, \tilde{k}_n, \tilde{k}_t$. Fig. 2a the curves $\left(\tilde{\Delta}_n, \tilde{a}\right)$ are plotted for fixed values of the stiffness $\tilde{k}_n = 1$, $\tilde{k}_t = 2$ and by varying the reversible tangential displacement $\tilde{\Delta}_{t,rev} = [0, 0.5, 7.1, 8.7, 10]$. For $\tilde{\Delta}_{t,rev} = 0$ the shearing force vanishes and a classical JKR curve is obtained. By increasing $\tilde{\Delta}_{t,rev}$ the effective work of adhesion $\tilde{G}_{I,eff}$ is reduced and, for a given $\tilde{\Delta}_n$, the contact area decreases. By using the condition (22) we have also plotted the limit curve for which $\tilde{G}_{I,eff} = 0$ (dot dashed black line). In panel (b) the effect of varying the normal stiffness $\tilde{k}_n = [0, 0.5, 1, 3, +\infty]$ for $\tilde{k}_t = 2, \tilde{\Delta}_{t,rev} = 0$ is shown. For vanishing normal stiffness $\left(\tilde{k}_n = 0\right)$ the contact radius does not depend on the remote displacement $\tilde{\Delta}_n$ and it's equal to that given by the JKR theory under vanishing normal load, i.e. $\tilde{a} = \tilde{a}_{P=0} = (9\pi/2)^{1/3}$, $\forall\ \tilde{\Delta}_n$. Regardless of the normal stiffness $\tilde{k}_n$ all the curves pass through the point $\mathrm{P}_0\left(\tilde{\Delta}_{n,P=0}, \tilde{a}_{P=0}\right)$, with $\tilde{\Delta}_{n,P=0} = \tilde{a}^2_{P=0}/3$ (Fig. 2b), where the normal force transmitted to the contact vanishes. For $\tilde{\Delta}_n > \tilde{\Delta}_{n,P=0}$, the normal load tranferred to the contact is compressive, hence, for a given $\tilde{\Delta}_n$, increasing the normal stiffness gives a larger contact radius. On the contrary for $\tilde{\Delta}_n < \tilde{\Delta}_{n,P=0}$ the normal load tranferred to the contact is tensile, hence, for a given $\tilde{\Delta}_n$, increasing the normal stiffness gives a smaller contact radius (see the stable branches in Fig. 2cb). Notice that by decreasing the normal stiffness the critical normal displacement $\tilde{\Delta}_{n,c}$ at which the system loses its stability decreases (black dots in Fig. 2). In panel (c) for given $\tilde{k}_n = 1$, and $\tilde{\Delta}_{t,rev} = 3$ the tangential stiffness is increased $\tilde{k}_t = [0, 1, 4, 12, +\infty]$. The $\tilde{\Delta}_n$ vs $\tilde{a}$ curves are bounded by two limits: the first is obtained for $\tilde{k}_t = 0$ and corresponds to the classical JKR solution, the second for $\tilde{k}_t = +\infty$ corresponds to the case when the tangential displacement is directly applied to the sphere hence $\tilde{\Delta}_{t,rev} = \sqrt{\lambda}\tilde{\Delta}_t = \sqrt{\lambda}\tilde{u}$.

In Fig. 3(abc) the curves contact radius $\tilde{a}$ versus the reversible tangential displacement $\tilde{\Delta}_{t,rev}$ are plotted for different values of normal displacement, tangential and normal stiffness. Panel (a) shows the contact radius shrinking for $\tilde{k}_t = 1, \tilde{k}_n = 1$ and different normal displacement $\tilde{\Delta}_n = [0, 5, 10, 15]$. Clearly the higher the normal load applied on the contact the higher the initial contact radius at $\tilde{\Delta}_{t,rev} = 0$. By solving Eq. (38), (39) one obtains the instability boundary that is plotted as a black dashed curve in panels Fig. 3(abc). Notice that those coincides with the simple condition $\partial\tilde{\Delta}_n/\partial\tilde{a} = 0$ (for more details see the Appendix - B). In Fig. 3b the curves $\tilde{a}$ vs $\tilde{\Delta}_{t,rev}$ are shown for $\tilde{\Delta}_n = 4$, $\tilde{k}_n = 1$ and by varying $\tilde{k}_t = [0, 0.5, 1, 2, 4, +\infty]$. Increasing the tangential stiffness $\tilde{k}_t$ the contact radius $\tilde{a}$ decreases faster, as a greater tangential load is transmitted to the interface, while at $\tilde{\Delta}_{t,rev} = 0$ all the curves coincide as the shearing load transmitted to the contact vanishes ($\tilde{\Delta}_t = 0$) or the modes are uncoupled ($\lambda = 0$). All the curves at different $\tilde{k}_t$ are bounded between the two limits of $\tilde{k}_t = 0$ (no shrinking) and $\tilde{k}_t \to +\infty$, which corresponds to the brittle model of Savkoor and Briggs (1977). In Fig. 3c we used $\tilde{k}_t = 1$, $\tilde{\Delta}_{t,rev} = 4$ and $\tilde{k}_n = [0, 0.5, 1, 2, 4, +\infty]$. Similarly to panel (b) the curves $\tilde{a}$, vs $\tilde{\Delta}_{t,rev}$ are bounded between two limits: for $\tilde{k}_n = 0$ the normal load acting on the contact patch is zero, so that $\tilde{a}\left(\tilde{\Delta}_{t,rev} = 0\right) = \tilde{a}_{P=0}$, while for $\tilde{k}_n = +\infty$ the remote displacement is equal to the sphere indentation $\tilde{\Delta}_n = \tilde{v}$. Notice that the normal displacement $\tilde{\Delta}_n$ and the normal load $\tilde{P}$ are related by Eq. (3) hence by keeping $\tilde{\Delta}_n$ constant the normal load would vary while the contact radius is shrinking.

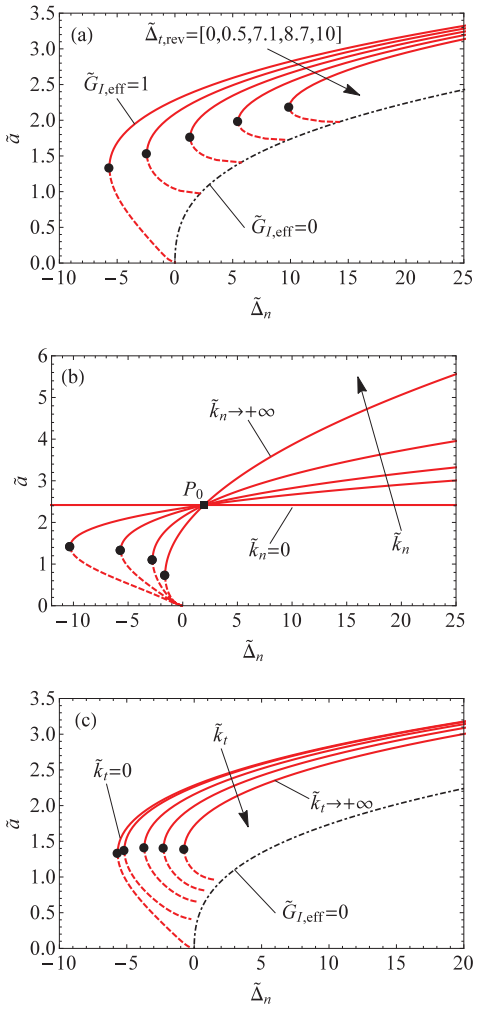

Fig. 2. Contact radius $\tilde{a}$ as a function of the imposed normal displacement $\tilde{\Delta}_n$ with (a) $\tilde{k}_n = 1, \tilde{k}_t = 2$, $\tilde{\Delta}_{t,rev} = [0, 0.5, 7.1, 8.7, 10]$, (b) $\tilde{k}_n = [0, 0.5, 1, 3, +\infty]$, $\tilde{k}_t = 2$, $\tilde{\Delta}_{t,rev} = 0$, (c) $\tilde{k}_t = [0, 1, 4, 12, +\infty]$, $\tilde{k}_n = 1, \tilde{\Delta}_{t,rev} = 3$. Solid (dashed) lines are used to mark the stable (unstable) solutions. In panels (a) and (c) the dot-dashed line indicates the boundary where $\tilde{G}_{I,eff} = 0$.

Fig. 4 shows a contour plot of the effective work of adhesion $\tilde{G}_{I,eff}$ (Eq. (20)) as a function of the tangential stiffness $\tilde{k}_t$ and of the reversible tangential displacement $\tilde{\Delta}_{t,rev}$, for $\tilde{a} = 1$. The map shows that for vanishing $\left(\tilde{k}_t, \tilde{\Delta}_t\right)$ the effective work of adhesion $\tilde{G}_{I,eff} \to 1$ as there is no effect of the shearing load, while $\lim_{\tilde{k}_t \to +\infty} \tilde{G}_{I,eff} = 1 - \tilde{\Delta}^2_{t,rev}/(3\pi\tilde{a})$ and condition (21) marks the boundary above which no adhesive solution exists.

Finally, by solving Eq. (38),(39) we look at the critical state (the instability point) in terms of critical contact radius a_c, critical normal force P_c and corresponding effective work of adhesion $G_{I,eff}$, for $\tilde{\Delta}_{t,rev} = 3$ (Fig. 5, left column, panels (a,c,e)) and $\tilde{\Delta}_{t,rev} = 4$ (Fig. 5, right column, panels (b,d,f)). In Fig. 5ab we plot the dimensionless critical normal force $\widehat{P}_c = \tilde{P}_c/\tilde{P}_{JKR,L}$, where $\tilde{P}_{JKR,L} = -(3/2)\pi$ is the pull-off force for the JKR model in load control. Fig. 5ab shows that for vanishing tangential and normal stiffness $\widehat{P}_c \to 1$, as the system reduces to classical JKR model in load control. By increasing $\tilde{k}_n$, for vanishing $\tilde{k}_t$, the critical normal load $\widehat{P}_c$ decreases and tends to $\tilde{P}_{JKR,\Delta}/\tilde{P}_{JKR,L} \simeq 0.556$, being $\tilde{P}_{JKR,\Delta} = -(5/6)\pi$ the JKR pull-off force in displacement control. Notice that in both panels (a,b) increasing $\tilde{k}_t$ leads to a reduction of the normal load that eventually may bring the critical normal force in the compressive region (in panels (b,d,f) compressive critical solutions are drawn with a red line). In the latter case, beyond the critical state, transition to sliding is expected, conversely, for tensile critical loads, a transition to separation is expected. Further for compressive normal loads the critical state is barely influenced by $\tilde{k}_n$ (see the region at $\widehat{P}_c < 0$ in Fig. 5b). Fig. 5cd shows instead the ratio $\widehat{a}_c = \tilde{a}_c/\tilde{a}_{JKR,L}$, being $\tilde{a}_{JKR,L} = (9\pi/8)^{1/3}$ the critical contact radius in the JKR model under load control. Panels (c,d) show that for vanishing normal stiffness $\widehat{a}_c$ is weakly influenced by $\tilde{k}_t$, while in the limit of high normal and weak tangential stiffness $\widehat{a}_c$ tends to $\tilde{a}_{JKR,\Delta}/\tilde{a}_{JKR,L} \simeq 0.481$, being $\tilde{a}_{JKR,\Delta} = (\pi/8)^{1/3}$ the critical contact radius in the JKR model under displacement control. Panels (c,d) show that increasing $\tilde{k}_t$ leads to a reduction

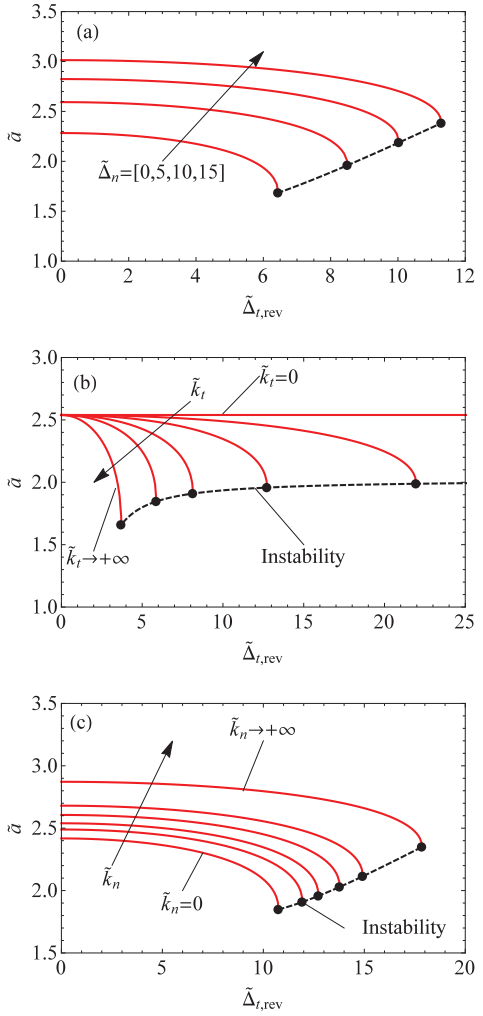

Fig. 3. Contact radius $\tilde{a}$ as a function of the reversible tangential displacement $\tilde{\Delta}_{t,rev}$ with (a) $\tilde{\Delta}_n = [0, 5, 10, 15]$, $\tilde{k}_t = 1, \tilde{k}_n = 1$, (b) $\tilde{\Delta}_n = 4$, $\tilde{k}_n = 1, \tilde{k}_t = [0.5, 1, 2, 4, +\infty]$, (c) $\tilde{k}_n = [0, 0.5, 1, 2, 4, +\infty]$, $\tilde{k}_t = 1, \tilde{\Delta}_{t,rev} = 4$. Solid (dashed) lines are used to mark the stable (unstable) solutions. The black dashed lines indicate the stability boundary.

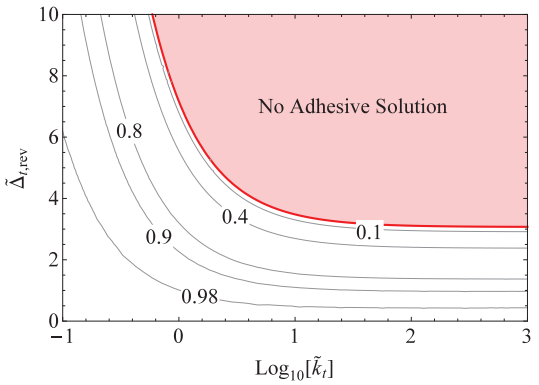

Fig. 4. Countour plot showing the effective work of adhesion $\tilde{G}_{I,eff}$ as a function of the tangential stiffness $\tilde{k}_t$ and the tangential displacement $\tilde{\Delta}_{t,rev}$, for $\tilde{a} = 1$.

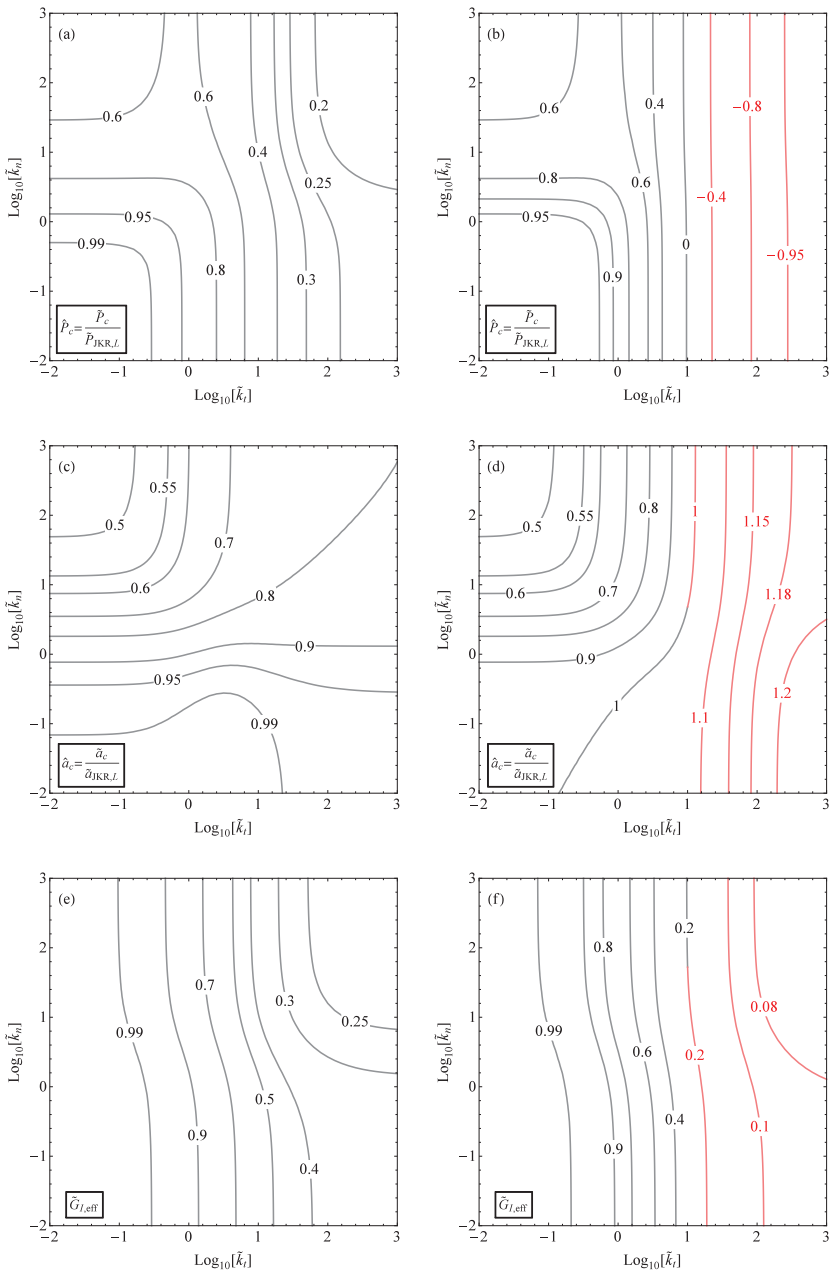

Fig. 5. Normal force $\hat{P}_c = \tilde{P}_c/\tilde{P}_{JKR,L}$ (a,b), contact radius $\hat{a}_c = \tilde{a}_c/\tilde{a}_{JKR,L}$ (c,d) and corresponding effective work of adhesion $\tilde{G}_{Ieff}$ (e,f) at the instability point for $\tilde{\Delta}_{t,rev} = 3$ (left column) and for $\tilde{\Delta}_{t,rev} = 4$ (right column) as a function of $(\tilde{k}_n, \tilde{k}_t)$ in log scale. In panels (b,d,f) red contours are used for compressive solutions $(\hat{P}_c < 0)$. (For interpretation of the references to color in this figure legend, the reader is referred to the web version of this article.)

of the contact radius, which is stronger for tensile than for compressive lodas. Finally, panels (e,f) show the effective surface energy $\tilde{G}_{I,eff}$. It is shown that $\tilde{G}_{I,eff}$ is strongly influenced by $\tilde{k}_t$, while it is weakly affected by $\tilde{k}_n$.We notice that, at the critical state $\tilde{G}_{I,eff} > 0$ also in the compressive region (red contours in Fig. 5f), which implies that the contact radius at the critical point is larger than the corresponding Hertzian adhesiveless solution for the same normal load.

5. Conclusions

In this work, we have studied the equilibrium solutions for a soft adhesive sphere that is loaded by imposing a remote displacement to the free ends of a normal and tangential spring. The model is developed under the assumption of short-range adhesion hence the contact patch is treated as an external crack that shrinks remaining circular under mode-mixity

loading conditions. The problem can be rewritten by introducing an effective work of adhesion which depends on both the tangential displacement imposed and the stiffness. In particular for vanishing lateral stiffness k_t no lateral forces are transmitted to the interface hence the problem reduces to the classical JKR solution under displacement control. On the other hand if the lateral stiffness becomes very rigid ($k_t \to +\infty$) the model reduces to the seminal model of Savkoor and Briggs (1977) when, additionally, we assume $\lambda = 1$ (brittle limit). The condition for the equilibrium solutions to be stable has been derived in general for fixed remote displacements. The model shows that for a given tangential displacement, the critical normal load, contact radius and corresponding effective work of adhesion depend weakly on the normal and strongly on the tangential stiffness. Eventually, for fixed normal/tangential displacements, increasing the tangential stiffness may lead the instability point to fall into the compressive region, suggesting a transition to sliding rather than separation. The model was derived including a mode-mixity function (previously validated against experimental results (Papangelo and Ciavarella, 2019)), which could take into account the variation of the interfacial toughness under mode-mixity conditions so that it could be very easy to adapt the model to fit or predict experimental results.

Declaration of Competing Interest

The authors declare that they have no known competing financial interests or personal relationships that could have appeared to influence the work reported in this paper.

CRediT authorship contribution statement

A. Papangelo: Conceptualization, Methodology, Validation, Formal analysis, Writing - original draft. **G. Cricrì:** Methodology, Supervision, Writing - review & editing. **M. Ciavarella:** Supervision, Writing - review & editing.

Acknowledgements

MC and AP acknowledge the support by the Italian Ministry of Education, University and Research under the Programme Department of Excellence Legge 232/2016 (Grant No. CUP-D94I18000260001). A.P. is thankful to the DFG (German Research Foundation) for funding the project PA 3303/1-1. A.P. acknowledges support from PON Ricerca e Innovazione 2014-2020-Azione I.2 - D.D. n. 407, 27/02/2018, bando AIM (Grant No. AIM1895471).

Appendix A. Alternative derivation using the concept of SIFs

In this analysis the contact patch is treated as an external crack under mixed-mode loading. Mode I is due to the adhesive interactions and is inherent in the JKR model, while the contributions of mode II (in plane shearing) and mode III (anti-plane shearing) are due to the tangential load applied (see Fig. 1b). On the periphery of the contact circle the three fractures modes combine. In particular defining θ the angle between the radius vector and the direction of T, we have that the energy release rate G is

$$G = \frac{1}{2E^*}\left[K_I^2 + K_{II\theta}^2 + \frac{1}{1-\nu}K_{III\theta}^2\right] \tag{40}$$

$$K_{II\theta} = \frac{T}{2a\sqrt{\pi a}}\cos(\theta); \quad K_{III\theta} = \frac{T}{2a\sqrt{\pi a}}\sin(\theta); \tag{41}$$

K_I, $K_{II\theta}$, $K_{III\theta}$ are respectively the stress intensity factors in mode I, II and III. There is very little evidence in the literature on how to combine the modes, hence we follow previous Literature results (Savkoor and Briggs, 1977; Waters and Guduru, 2010)) that suggest to make an average of the mode II and mode III around the periphery so that the circumferential averaged energy release rate is

$$G = \frac{1}{2E^*}\left[K_I^2 + \frac{2-\nu}{2(1-\nu)}K_{II}^2\right] \tag{42}$$

where for $\nu = 1/2$, $\frac{2-\nu}{2(1-\nu)} = \frac{3}{2}$. For mode I, the stress intensity factor is given by

$$K_I = \frac{P_a}{2a\sqrt{\pi a}} = \frac{P_H - P}{2a\sqrt{\pi a}} \tag{43}$$

where we have split the total load $P = P_H - P_a$ into two contributions: a compressive Hertzian load $P_H = \frac{4E^*a^3}{3R}$ and a Boussinesq flat punch solution with total load P_a that is responsible of the contact edge singularity.

For mode II, the stress intensity factor K_{II} along the shearing direction is given by

$$K_{II} = \frac{T}{2a\sqrt{\pi a}} \tag{44}$$

As in the main text, to account for interfacial dissipative effects, we write the equilibrium condition according to the proposed mode-mixity model (15), hence

$$\frac{1}{2E^*}\left[K_I^2+\frac{3}{2}\lambda K_{II}^2\right]=G_{Ic} \tag{45}$$

where G_{Ic} is the interface toughness in mode I (or "surface energy"). Using Eq. (45),(44,43), the equilibriumg equation gives

$$P=\frac{4E^*a^3}{3R}-\sqrt{8\pi E^*a^3G_{Ic}-\frac{3}{2}\lambda T^2}$$

Substituting in the latter the expressions for the normal load (Eq. (3)) and the tangential load (Eq. (5)) as a function of the normal and tangential displacement imposed (Δ_n, Δ_t) leads to

$$\Delta_n=\left(\frac{1}{k_n}+\frac{1}{2aE^*}\right)\left[\frac{4E^*a^3}{3R}-\sqrt{8E^*a^3\pi\left(G_{Ic}-\lambda\frac{E^*}{3\pi a}\frac{\Delta_t^2}{\left(1+\frac{4}{3}\frac{E^*a}{k_t}\right)^2}\right)}\right]+\frac{a^2}{3R} \tag{46}$$

which coincides with Eq. (19).

Appendix B. Practical considerations on the instability points

In order to evaluate the stability of a solution for imposed external displacements Δ_n, Δ_t we have written in the main text (Eq. (25))

$$\frac{\partial G_{rev}}{\partial A}>0 \tag{47}$$

Eq. (18) gives the equilibrium solution in terms of the contact radius a, given the displacements Δ_n, Δ_t. We can write the latter also in terms of a pseudo-time variable τ

$$a=a(\tau);\quad \Delta_n=\Delta_n(\tau);\quad \Delta_t=\Delta_t(\tau); \tag{48}$$

Indicating as usual the time derivative with a dot, in the equilibrium points we have

$$\frac{\partial G_{rev}}{\partial a}\dot{a}+\frac{\partial G_{rev}}{\partial \Delta_n}\dot{\Delta}_n+\frac{\partial G_{rev}}{\partial \Delta_t}\dot{\Delta}_t=0 \tag{49}$$

In the critical condition for stability, with external displacement as imposed, we have

$$\frac{\partial G_{rev}}{\partial A}=0\leftrightarrow\frac{\partial G_{rev}}{\partial a}=0 \tag{50}$$

which permits to obtain

$$\frac{\partial G_{rev}}{\partial \Delta_n}\dot{\Delta}_n+\frac{\partial G_{rev}}{\partial \Delta_t}\dot{\Delta}_t=0 \tag{51}$$

which, in general, is verified when along the loading path $\dot{\Delta}_n=\dot{\Delta}_t=0$, which for $\dot{a}\neq 0$, also implies that

$$\frac{\partial \Delta_n}{\partial a}=0;\quad \frac{\partial \Delta_t}{\partial a}=0 \tag{52}$$

The latter condition explains why at the critical point of stability $\partial\Delta_n/\partial a$ and $\partial\Delta_t/\partial a$ vanish almost always and provide a useful condition to determine the critical point of stability. The exception is represented by the particular case when $\dot{\Delta}_n\neq 0$ and $\dot{\Delta}_t\neq 0$, and Eq. (51) is verified if

$$\frac{\partial G}{\partial \Delta_n}\dot{\Delta}_n=-\frac{\partial G}{\partial \Delta_t}\dot{\Delta}_t \tag{53}$$

but the last condition is not generally verified at any point in the equilibrium path, except if that is a bifurcation point.

References

Argatov, I., Papangelo, A., 2019. Axisymmetric JKR-type adhesive contact under equibiaxial stretching. J. Adhes. 1–15. doi:10.1080/00218464.2019.1646648.
Argatov, I., Papangelo, A., Ciavarella, M., 2020. Elliptical adhesive contact under biaxial stretching. Proceedings of the Royal Society A 476 (2233). 20190507
Bhushan, B., Israelachvili, J.N., Landman, U., 1995. Nanotribology: friction, wear and lubrication at the atomic scale. Nature 374 (6523), 607.
Cao, H.C., Evans, A.G., 1989. An experimental study of the fracture resistance of bimaterial interfaces. Mech. Mater. 7 (4), 295–304.
Ciavarella, M., 2018. Fracture mechanics simple calculations to explain small reduction of the real contact area under shear. Facta Univ. Ser. 16 (1), 87–91.
Ciavarella, M., Joe, J., Papangelo, A., Barber, J.R., 2019. The role of adhesion in contact mechanics. J. R. Soc. Interface 16 (151), 20180738.
Ciavarella, M., Papangelo, A., 2017. Discussion of "measuring measuring and understanding contact area at the nanoscale: A review review"(Jacobs, TDB, and ashlie martini, a., 2017. ASME Appl. Mech Mech. Rev. 69 (6). P. 060802). Applied Mechanics Reviews, 69(6), 065502
Ciavarella, M., Papangelo, A., Afferrante, L., 2017. Adhesion between self-affine rough surfaces: possible large effects in small deviations from the nominally Gaussian case. Tribol. Int. 109, 435–440.
Da Silva, L.F.M., Öchsner, A., 2008. Modeling of Adhesively Bonded Joints. Springer, Berlin.

Heim, L.O., Blum, J., Preuss, M., Butt, H.J., 1999. Adhesion and friction forces between spherical micrometer-sized particles. Phys. Rev. Lett. 83 (16), 3328.
Homola, A.M., Israelachvili, J.N., McGuiggan, P.M., Gee, M.L., 1990. Fundamental experimental studies in tribology: the transition from "interfacial" friction of undamaged molecularly smooth surfaces to "normal" friction with wear. Wear 136 (1), 65–83.
Hutchinson, J.W., 1990. Mixed mode fracture mechanics of interfaces. Metal-Ceram. Interfaces 4, 295–306.
Hutchinson, J.W., Suo, Z., 1992. Mixed mode cracking in layered materials. In: Hutchinson, J.W., Wu, T.Y. (Eds.), In Advances in applied mechanics, vol. 29. Academic Press, Boston, MA. 63–191
Johnson, K.L., 1985. Contact Mechanics. Cambridge University Press, Cambridge. Doi:10.1017/CBO9781139171731
Johnson, K.L., 1996. Continuum mechanics modeling of adhesion and friction. Langmuir 12, 4510–4513.
Johnson, K.L., 1997. Adhesion and friction between a smooth elastic spherical asperity and a plane surface. Proc. R. Soc. Lond. A 453 (1956), 163–179.
Johnson, K.L., Greenwood, J.A., 2005. An approximate JKR theory for elliptical contacts. J. Phys. D 38 (7), 1042.
Johnson, K.L., Kendall, K., Roberts, A.D., 1971. Surface energy and the contact of elastic solids. Proc. R. Soc. Lond. A 324, 301–313.
Lengiewicz, J., de Souza, M., Lahmar, M., Courbon, C., Dalmas, D., Stupkiewicz, S., Scheibert, J., 2020. Finite deformations govern the anisotropic shear-induced area reduction of soft elastic contacts. arXiv:2005.02107
Maugis, D., 2000. Contact, Adhesion and Rupture of Elastic Solids. Springer, New York.
McMeeking, R.M., Ciavarella, M., Cricri, G., Kim, K.S., 2020. The interaction of frictional slip and adhesion for a stiff sphere on a compliant substrate. J. Appl. Mech. 87 (3).
Mergel, J.C., Sahli, R., Scheibert, J., Sauer, R.A., 2018. Continuum contact models for coupled adhesion and friction. J. Adhes. doi:10.1080/00218464.2018.1479258.
Mergel, J. C., Scheibert, J., Sauer, R. A., 2020. Contact with coupled adhesion and friction: Computational framework, applications, and new insights. arXiv:2001.06833
Papangelo, A., Ciavarella, M., 2019. On mixed-mode fracture mechanics models for contact area reduction under shear load in soft materials. J. Mech. Phys. Solids 124, 159–171.
Papangelo, A., Scheibert, J., Sahli, R., Pallares, G., Ciavarella, M., 2019. Shear-induced contact area anisotropy explained by a fracture mechanics model. Physical Review E 99 (5), 053005.
Pelesko, J.A., Bernstein, D.H., 2002. Modeling Mems and Nems. CRC press.
Sahli, R., Pallares, G., Ducottet, C., Ben Ali, I.E., Al Akhrass, S., Guibert, M., Scheibert, J., 2018. Evolution of real contact area under shear. Proc. Natl. Acad. Sci. 115 (3), 471–476. doi:10.1073/pnas.1706434115.
Sahli, R., Pallares, G., Papangelo, A., Ciavarella, M., Ducottet, C., Ponthus, N., Scheibert, J., 2019. Shear-induced anisotropy in rough elastomer contact. Phys. Rev. Lett. 122 (21), 214301.
Savkoor, A.R., Briggs, G.A.D., 1977. The effect of a tangential force on the contact of elastic solids in adhesion. Proc. R. Soc. Lond. A 356, 103–114.
Waters, J.F., Guduru, P.R., 2010. Mode-mixity-dependent adhesive contact of a sphere on a plane surface. Proc. R. Soc. A 466, 1303–1325.